SCC3 acts as the cohesin and inhibits inter-sister chromatids repair during rice meiosis

Yangzi Zhao[1, 3], Lijun Ren[1, 3], Tingting Zhao[1, 3], Hanli You[1], Yonjie Miao[1], Huixin Liu[1], Lei Cao[1], Bingxin Wang[1], Yi Shen[1], Yafei Li[1], Ding Tang[1], Zhukuan Cheng[1, 2, *]

[1] State Key Lab of Plant Genomics, Institute of Genetics and Developmental Biology, Innovation Academy for Seed Design, Chinese Academy of Sciences, 100101 Beijing, China

[2] Jiangsu Key Laboratory of Crop Genomics and Molecular Breeding/Key Laboratory of Plant Functional Genomics of the Ministry of Education, Jiangsu Co-Innovation Center for Modern Production Technology of Grain Crops, Yangzhou University, Yangzhou 225009, China.

[3] These authors contribute equally to this work: Yangzi Zhao, Lijun Ren, Tingting Zhao.

[*] **Corresponding author: Zhukuan Cheng, Email: zkcheng@genetics.ac.cn;**

Telephone: 0086-10-6480, 6551

Fax: 0086-10-6480, 6595

Abstract

Cohesin is a multi-subunit protein responsible for holding sister chromatids together during mitosis and meiosis. Each subunit is functionally essential, and their deletion is always lethal. SCC3 is a highly conserved constituent of the cohesin complex. However, the exact mitotic and meiotic functions of SCC3 in rice remains to be elucidated. Here, we found null alleles of *SCC3* cause embryo lethality. Only *scc3* weak mutants could survive and show vegetative and reproductive defects. Specifically, the replication process of sister chromatids is disturbed in *scc3* during interphase both in mitosis and meiosis. Moreover, SCC3 has distinct localization patterns between mitotic and meiotic cells. The numbers of DMC1, RAD51 and ZIP4 foci are significantly decreased in *scc3*, and ZEP1 displays as an abnormal punctate foci during zygotene. Importantly, the *scc3* fails to synapse, but in this case chromosome fragmentation is absent. Thus, SCC3 seems to inhibit inter-sister chromatids repair (ISR), and this process is independent of DMC1-mediated ISR.

Keywords: rice, cohesin complex, inter-sister chromatids repair, meiosis, mitosis

Introduction

The correct segregation of sister chromatids is essential for mitotic cell stabilization and to generate haploid gametes during meiosis. The cohesin complex is a conserved multi-subunit protein system that guarantees the proper segregation of sister chromatids in mitosis and across living organisms. This complex is formed by four core subunits, including the structural maintenance of chromosomes (SMC) subunits SMC1 and SMC3, and the sister chromatid cohesin (SCC) subunits SCC1 and SCC3 (Bolanos-Villegas et al., 2017; Moronta-Gines et al., 2019). The cohesin complex forms a ring encircling the sister chromatids and ensures genomic stability during DNA replication (Higashi et al., 2020). In addition, cohesin also participates in the repair of DNA double-strand breaks (DSB), homologous pairing, construction of the synaptonemal complex (SC), orientation of kinetochores, and regulation of gene expression (Nasmyth and Haering, 2009).

Cohesin is established during the S phase, and includes arm and centromeric cohesin. Arm cohesin ensures sister chromatids bond together during mitotic prophase. Centromeric cohesin persists until the metaphase-to-anaphase transition, and is vital to resist the force exerted by spindle microtubules, allowing for the accurate segregation of sister chromatids to opposite poles of the cell. The dissociation of cohesin generally occurs in two steps, including through the dissociation of cohesin on chromosome arms during prometaphase, followed by the degradation of cohesin at the centromeres at the onset of anaphase (Ishiguro and Watanabe, 2007; Watanabe, 2005). This allows sister chromatids to segregate in mitosis.

Meiosis contains a single round of DNA replication, but, in contrast to mitosis, is followed by two successive chromosome divisions. Nonetheless, while the loading mechanism of cohesin is very similar to the analogous process during mitosis, the cohesin degradation during meiosis occurs in two steps: from chromosome arms

during the first meiotic division, and from the centromeres during the second meiotic division (Mercier et al., 2015). During meiosis I, homologous chromosomes are linked by chiasmata that separate at metaphase I. At this stage, cohesin dissociates from chromosome arms while the two sister chromatids remain closely together because centromeres cohesin are preserved. Subsequently, the sister chromatids separate at anaphase II due to full cohesin disassociation at the chromosome arms and centromeres. During this process, sister chromatids cohesin is protected by shugoshin from cleavage by separase (Wang et al., 2012; Wang et al., 2011), which determines the correct separation of sister chromatids during meiosis.

Notably, the cohesin complex plays additional functional roles in meiosis. Specifically, cohesin on chromosome arms is crucial for normal progression of meiosis I, while centromeric cohesin plays a more prominent role in meiosis II by geometrically orientating the sister chromatids. During meiosis I, homologous chromosomes are segregated in opposite directions to halve the chromosome number, but sister chromatids remain temporarily mono-oriented and move to the same pole. In meiosis II, sister chromatid pairs become bi-oriented and separate towards opposite spindle poles through similar mechanisms as those observed in mitosis (Schvarzstein et al., 2010). In this process, centromeric cohesin plays a crucial role in establishing kinetochore geometry and thus determining sister kinetochore orientation (Gryaznova et al., 2021). In addition, the cohesin complex impacts the formation of chromosome axial elements (AE) and the assembly of the synaptonemal complex (SC) (Agostinho et al., 2016; Fujiwara et al., 2020; Llano et al., 2012). Besides, the cohesin complex regulates gene expression in eukaryotes, acting as a transcriptional co-activator in humans that is recruited by sequence-specific transcription factors (Casa et al., 2020; Kagey et al., 2010; Lara-Pezzi et al., 2004; Remeseiro et al., 2012). Finally, the cohesin complex is now emerging as a key player in DSBs repair pathway choice and efficiency. In yeast, cohesin and DMC1 may interactively modulate homologous recombination partner choice, with program-appropriate effects (Hong et al., 2013; Phipps and Dubrana, 2022; Sanchez-Moran et al., 2007).

To date, there were many researches on cohesin subunits, which had different functions throughout the cell cycle. In yeast, SCC1 ensures sister chromatid cohesin in mitosis and is associated with chromosomes during the S phase, dissociating during the metaphase-to-anaphase transition. The expression of SCC1 gradually decreases at the beginning of meiosis, whereby SCC1 likely plays a minor role during meiosis (Michaelis et al., 1997). Instead, REC8 is a special meiotic-specific cohesin component that replaces SCC1 in yeast (Klein et al., 1999; Watanabe and Nurse, 1999) and which is expressed in leptotene and decreases after pachytene (Shao et al., 2011). REC8 also plays a crucial role establishing sister kinetochore orientation in yeast, mice and plants (Chelysheva et al., 2005; Ogushi et al., 2021; Toth et al., 2000). In addition, *rec8* mutants in flowering plants exhibit sticky chromosomes, which severely affects the localization of other key meiotic proteins (Cai et al., 2003; Chelysheva et al., 2005; Shao et al., 2011). Moreover, SCC3-SCC1 subcomplex is necessary for cohesin loading and the establishment of sister chromatid cohesin in mitosis in yeast (Li et al., 2018a; Orgil et al., 2015). SCC3 also being responsible for maintaining centromeric orientation during meiosis in *Arabidopsis* (Cai et al., 2003; Chelysheva et al., 2005; Kulemzina et al., 2012). Taken together, these results indicated that cohesin is crucial for the stability of chromosome structure in mitosis and meiosis. However, does cohesin have other functions? such as participating in homologous recombination and DSBs repair process? Also, the mechanisms through which SCC3 regulates the assembly of sister chromatid cohesin in mitosis and its function in meiosis were not well investigated. SCC3 and REC8 are both meiotic cohesin, and what is the difference between them?

Here, we further investigated SCC3 functions, demonstrating its involvement in mitosis and meiosis. We observed the replication process of chromosome 12 during interphase confirming that SCC3 stabilizes chromosome replication process both in mitosis and meiosis, which is crucial for sister chromatids cohesin. Furthermore, we investigated the process of cohesin loading and degradation on chromosomes by using the antibody of SCC3 on chromosomes during mitosis and meiosis. We also show the

localization of SCC3 is regulated by REC8. Meanwhile, other meiotic proteins (COM1, DMC1, RAD51, PAIR2 and PAIR3) failed to localize in *rec8*. That is, REC8 is a fundamental meiotic protein which is prerequisite for the localization of other meiotic proteins. However, the meiotic components (DMC1, RAD51, ZIP4, HEI10 and ZEP1) could be present in *scc3* but apparently making no functional contribution to recombination and synapsis indicating that SCC3 participates in homologous pairing, synapsis, recombination progress and CO formation. More importantly, we found meiotic DSBs were well repaired in *scc3*, probably using sister chromatids as a template, which means SCC3, as a member of cohesin complex, could inhibit inter-sister chromatids repair during meiosis. Finally, we explore different roles of SCC3 and REC8 in meiosis. All findings are integrated into a coherent model.

Results

SCC3 causes both vegetative and reproductive growth defects

We performed a BLAST search in the Rice Genome Annotation Project database (http://rice.plantbiology.msu.edu/cgibin/gbrowse/rice) and found a single hypothetical homologue of SCC3 proteins (*A. thaliana* SCC3, *M. musculus* STAG3 and *H. sapiens* SA1). This candidate protein is encoded by the *Os05g0188500* gene and shares the highest similarity with *AtSCC3*. The full-length cDNA of *SCC3* is 3755 nucleotides long and comprises 22 exons and 21 introns. SCC3 contains a 3345-nucleotide-long ORF that encodes a 1116aa protein. In higher eukaryotes, SCC3 is an evolutionary conserved protein that contains a highly conserved STAG domain (140-239aa), as predicted by SMART (Figure S1A). Multiple alignments of full-length SCC3 protein sequences and its homologs in other plants revealed the STAG domain is highly conserved across both monocotyledons and dicotyledons (Figure S1B). Homology modeling indicated SCC3 protein structures are strongly conserved in different species, which also possess similar STAG domains (Figure S2A). Additionally, a phylogenetic tree was constructed with full-length SCC3 amino acid sequences that

145 confirmed this protein is conserved in eukaryotes (Figure S2B). We also did multiple
146 sequence alignments of these proteins used in the evolutionary tree analysis (Figure
147 S3).

148 A previous study in Arabidopsis (Chelysheva et al., 2005) identified a T-DNA
149 insertion at the boundary between intron 5 and exon 6 of *SCC3* that caused lethality,
150 whilst a weak allele was able to survive albeit with some developmental defects. To
151 clarify SCC3 function in rice, we used the CRISPR-Cas9 system to generate three
152 transgenic lines (Figure S4). The first allele (*scc3-1*) contains a frameshift "GA"
153 deletion in exon 2 and the second allele (*scc3-2*) contains a frameshift "ACCGA"
154 deletion in exon 11. We tested for allelism between these two *scc3* mutants by
155 crossing *scc3-1*$^{+/-}$ (male) and *scc3-2*$^{+/-}$ (female). Of the 78 F1 plants, 18 were *scc3-1*$^{+/-}$
156 , 26 were *scc3-2*$^{+/-}$, 34 were wildtype for both loci. Thus, these two mutants are allelic
157 and heterozygous *scc3-1/scc3-2* is lethal. We were unable to isolate homozygous
158 mutants in these two allelic progenies (n=128, 87 plants were *scc3-1*$^{+/-}$ and 41 were
159 wildtype; n=116, 80 plants were *scc3-2*$^{+/-}$ and 36 were wildtype). These results
160 suggested that *scc3-1* and *scc3-2* mutants were both embryo-lethal.

161 In addition, we obtained a weak transgenic line (*scc3*) containing a frameshift
162 "T" insertion in exon 19 leading to premature termination of translation (Figure S4).
163 We found the *scc3* weak mutant exhibits abnormal vegetative growth (Figures 1A and
164 1B), and thus proceeded with further investigation of its other phenotypic effects,
165 which revealed *scc3* decreases plant height, tiller number and panicle length (Figures
166 1C and S5B-S5D). To investigate the patterns of *SCC3* expression, we employed RT-
167 PCR in various tissues and found the gene is ubiquitously expressed, particularly in
168 roots, leaves and small panicles (Figure S5A). Accordingly, the weak mutant of SCC3
169 causes severe vegetative growth defects in rice plants.

170 To elucidate whether *SCC3* is involved in meiosis, we performed cytological
171 observation of anthers stained with 1% I_2-KI, and found almost all pollen grains were
172 shrunken and inviable (Figures 1D and S5E). Our results also showed *scc3* flowers

did not set seeds when pollinated with wild-type pollen, suggesting the mutant was sterile. We further observed heterozygous *scc3* plants produced progenies with a segregation ratio of 3:1 (normal: dwarf and sterile), indicating the *scc3* mutation is recessive and monogenic. These data suggest that *scc3* weak mutation dramatically interferes with plant vegetative and reproductive growth, which may be relevant to mitosis and meiosis.

SCC3 is required for sister chromatid cohesin during mitosis

To determine whether SCC3 is involved in sister chromatid cohesin in mitosis, we observed chromosome behavior in root tip cells of *scc3* and wildtype. DNA replicates and folds into an ordered structure during interphase in wildtype plants (Figure 1E). After this, the chromosomes condensed and formed short thread-like chromatids during prophase, which developed into further condensed sister chromatids in prometaphase that were aligned on the equatorial plate before separating to different poles of the cell.

In contrast, *scc3* exhibited "X"-shaped chromosomes with distant arms and telomeres in prometaphase (Figures 1E and 1G), indicating a loss of cohesin between sister chromatids. Approximately two-thirds of *scc3* root tip cells (70.6%, n=88) contained partially or completely separated sister chromatids (Figure 1H), which were loosely arranged on either side of the equatorial plate during the anaphase-to-telophase transition (Figure 1E), demonstrating the sister chromatids separated in advance as they were pulled to the spindle poles of the cell. But we did not observe any aneuploidy in anaphase, because mitotic tubulin was attached to centromeres of sister chromatids during prometaphase, and sister chromatids were still together at this time in *scc3*, which guarantee sister chromatids separated equally.

Furthermore, we monitored the distance between centromeres using FISH probes with centromere-specific tandem repetitive sequence CentO in both wildtype and *scc3* somatic cells during prometaphase. We found the distance between sister centromeres

also dramatically increased in *scc3* (Figure 1F, n=25). However, we also noted that, despite the distance between sister chromatids increased in *scc3* weak mutants, sisters were still observed side-by-side during prometaphase, suggesting that there may be other cohesin proteins to maintain sister chromatids associated. Our results demonstrated SCC3 is required for cohesin between sister telomeres, centromeres and arms during mitosis.

To explore whether SCC3 affects the replication process of sister chromatids, we performed full-length FISH assays to monitor the dynamic phenotype of chromosome 12 during interphase. In the wildtype, sister chromatids were replicating that could be observed during interphase (Figure 2A). Subsequently, two chromosome clumps formed during prophase and developed into high-order linear chromosomes during prometaphase. During this time, two sister chromatids seemed overlapped and condensed into a short stick. However, in *scc3* an obvious chromosomes fragmentation was observed during interphase, which means the replicating chromatids are abnormally organized. During prophase, chromosome 12 were still into a lump and unable to condense into a stick phenotype. In prometaphase, these abnormal chromosomes finally form loosely-connected sister chromatids (Figure 2A). These observations indicated that SCC3 is involved in the replication process of sister chromatids, which may be implicated as a regulator of the genome, influencing chromatin composition and dynamics, and crucially genome organization through folding chromosomes.

To investigate the localization of SCC3 during mitosis, we generated a mouse polyclonal antibody against C-terminal and performed immunostaining of root tip wildtype cells (Figure 2B). We noted no SCC3 signal was present in *scc3* root tip cells, confirming the specificity of the SCC3 antibody utilized in mitosis (Figure S6A). We found SCC3 was uniformly distributed in the cells during interphase in most cases. From interphase to prophase, as chromosome replication completed, the centromere signals became brighter and SCC3 signals also become denser and brighter. SCC3

eventually converged into intact chromosomes at prometaphase. From metaphase to telophase, SCC3 signal disappeared (Figure 2B). These observations suggested that SCC3 may enhance the interaction with DNA during the transition from interphase to prophase, and dissociated from chromosomes after prometaphase.

SCC3 acts as an axial element during meiosis

REC8 is a special axial protein indicating meiotic progression (Shao et al., 2011). To evaluate SCC3 localization in meiosis, we performed dual-immunolocalization between SCC3 and REC8 in wildtype meiocytes. REC8 signals were initially detected as foci in the nucleus at leptotene, while SCC3 was detectable simultaneously (Figure 3A). From leptotene to zygotene, SCC3 signals were detected as similar elongated foci that formed filamentous structures on the chromosomes. During pachytene and diplotene, constant SCC3 signals were distributed along chromosome axes (Figure 3A). At diakinesis, axial SCC3 signals became diffuse and centromeric signals gradually became clear. At metaphase I, only centromeres SCC3 antibody signals remained (Figure 3B). However, REC8 signals were difficult to detect from diakinesis to metaphase I (Figure S7). In order to further clarify the localization pattern between SCC3 and REC8, we performed super-resolution imaging (SIM) on wildtype meiocytes, which showed REC8 and SCC3 were parallel and colocalized forming parallel axial elements (Figure 3C). In addition, central elements ZEP1 formed two parallel lines surrounded by SCC3 signals (Figure 3D). We also noted no SCC3 signal was present in *scc3* meiocytes, confirming the specificity of the SCC3 antibody utilized in meiosis (Figure S6B).

SCC3 is required for sister chromatid cohesin in early meiosis

The interphase of meiosis is similar to mitosis, and sister chromatids replicate during interphase and are linked together by cohesin. To determine whether SCC3 is involved in sister chromatid cohesin during meiosis, we observed chromosome behaviors of meiocytes in *scc3* and wildtype before leptotene. Cytological phenotypes

of meiosis initiation in rice have been reported in detail (Zhao et al., 2018). The first meiotic stage that can be distinguished is preleptotene, and sister chromatids should have completed replication during this time. In preleptotene, the meiocytes chromosomes were discrete and partially contracted during preleptotene (Figure 4A), and subsequently formed thin threads in the wildtype at leptotene. In *scc3*, chromosomes at preleptotene exhibited dispersed appearance with blurred outlines. During leptotene, chromosomes maintained a loose shape and no filamentous threads were present. These observations indicate SCC3 participates in sister chromatids replication process in early meiosis.

We then examined chromosome behavior in *rec8* single mutants and *scc3 rec8* double mutants at preleptotene (Figure 4A). Unexpectedly, *rec8* exhibited elongated chromosomes similar to the wildtype, whereas *scc3 rec8* exhibited diffused chromosomes similar to *scc3*. These results indicate REC8 does not affect the early replication process of sister chromatids, and the chromosome defects in *scc3 rec8* double mutant may be caused by the mutation of SCC3. In addition, we performed full-length FISH assays to monitor chromosome 12 at preleptotene (Figure 4B), and found that replicated chromosome 12 can form short rod-shaped threads in both wildtype and *rec8*, but appears as a diffuse structure in *scc3* and *scc3 rec8* mutants due to abnormal replication process. These observations are consistent with DAPI staining results, further demonstrating SCC3 affects sister chromatid replication process in early meiosis.

Homologous chromosome pairing and synapsis are disturbed in *scc3*

To study the causes of sterility in *scc3*, we investigated male meiotic chromosome behavior of wildtype and *scc3* meiocytes. In the former, homologous chromosomes paired at early zygotene and fully synapsed at pachytene. Moreover, during metaphase I, 12 bivalents were orderly arranged on the equatorial plate, with homologous chromosomes separating at anaphase I (Figure 5A). In contrast, *scc3* chromosome behavior showed no differences at zygotene, with meiotic defects

283 becoming apparent at pachytene, when most chromosomes dispersed as single threads
284 with incomplete homologous paring (Figure 5A). We identified 24 univalents during
285 diakinesis and metaphase I (n=161, 150 meiocytes have 24 univalents, 11 meiocytes
286 have 1-2 bivalents), which were always pulled to opposite poles leading to sister
287 chromatids separation at anaphase I. However, in *spo11* mutants containing 24
288 univalents, sister chromatids were separated randomly or still linked together (Figure
289 S8A). These observations show SCC3 determine the separation of sister chromatids
290 during anaphase I, and is involved in homologous pairing, which could influence the
291 normal process of synapsis.

292 The telomere bouquet is a prerequisite for homologous pairing at early zygotene
293 (Zhang et al., 2020). We performed a FISH assay to detect bouquet formation in
294 wildtype and *scc3* meiocytes using a telomere-specific probe (pAtT4). As expected,
295 the wildtype telomeres were attached to a confined region, forming a typical bouquet
296 on the nuclear envelope at zygotene. Interestingly, the formation of telomere bouquets
297 also occurred normally in *scc3* (Figure S8B). We then used 5S rDNA to monitor
298 homologous pairing, and detected two overlapping 5S rDNA foci at pachytene in the
299 wildtype, but two separated 5S rDNA foci in unpaired homologous chromosomes in
300 *scc3* (n=52; Figure S8C), confirming SCC3's role in homologous pairing.

301 Homologous chromosomes align and then become closely juxtaposed by a
302 proteinaceous structure known as the synaptonemal complex (SC), which is
303 comprised of two parallel arrays of axial elements (AE), termed lateral elements (LE)
304 prior to synapsis, that form the structural basis for the assembly of the SC (Ren et al.,
305 2021). Since SCC3 is a LE component, we monitored the assembly of the SC through
306 immunostaining using an antibody against ZEP1 in *scc3* and wildtype meiocytes. In
307 the wildtype, we observed ZEP1 gradually elongated and formed short linear signals
308 during zygotene, which eventually extended along the paired homologous
309 chromosomes at pachytene (Figure 5B). However, *scc3* mutants displayed ZEP1 as a
310 few punctate foci during zygotene. These abnormal structures were also present at

311 pachytene (Figure 5B), suggesting SCC3 plays a crucial role in the assembly of the
312 SC. In addition, we also examined the localization of other LEs (PAIR2 and PAIR3),
313 and these proteins behave normally in *scc3* (Figure S9).

314 **_SCC3_ is essential for recombination progress and CO formation**

315 Since homologous pairing was impaired in *scc3* meiocytes, we wondered
316 whether recombination was normal in *scc3*. γH2AX is a marker that is used as a proxy
317 to monitor DNA DSBs. Therefore, we investigated the number of γH2AX foci to
318 explore the DSB formation. There was no significant difference in the number of
319 γH2AX foci between the wildtype and *scc3* (265.4 ± 8.6, n=31 for *scc3* meiocytes;
320 262.2 ± 7.2, n=20 for wildtype meiocytes) (Figure 6A). Additionally, we also
321 examined the DSB resection factor (COM1), meiotic strand-invasion and exchange
322 factors (RAD51, DMC1) and the Class I, interference-sensitive crossover (CO)
323 marker (ZIP4) in both wildtype and *scc3*. Immunostaining results revealed that the
324 number of COM1 foci (290.3 ± 8.8, n=26 for *scc3* meiocytes; 293.8 ± 9.4, n=23 for
325 wildtype meiocytes) were not significantly different between the wildtype and *scc3*
326 (Figures 6A and 6B). However, DMC1 (65.4 ± 17.1, n=25 for *scc3* meiocytes; 281.2
327 ± 8.3, n=20 for wildtype meiocytes), RAD51 (55 ± 21.7, n=26 for *scc3* meiocytes;
328 306 ± 11.9; n=24 for wildtype meiocytes) and ZIP4 (58 ± 17.9, n=23 for *scc3*
329 meiocytes; 316.6 ± 11.1, n=21 for wildtype meiocytes) foci were significantly
330 decreased in *scc3*, suggesting that recombination progress and CO formation was
331 disturbed in *scc3*. Previous studies revealed that HEI10 is a marker of Class I COs. In
332 wide type, prominent HEI10 foci were observed (24.2 ± 3.8, n=25) at late pachytene
333 (Figures 6A and 6B). By comparison, in *scc3* most HEI10 foci were sparse and did
334 not present as large bright signals. Taken together, these results suggested that CO
335 maturation was disturbed in *scc3*. Although recombinant proteins could be localized
336 in a small portion, the homologous recombination process was still greatly restricted.

337 **SCC3 inhibits inter-sister chromatids repair during meiosis**

It is worth noting that DSBs formation was normal in *scc3*, and inter-homolog strand-invasion is destabilized which leads to the defects in CO formation. Nevertheless, in *scc3*, the meiotic DSBs are reliably repaired as there is no chromosome fragmentation, most likely using sister chromatid as a repair template, leading to 24 univalents (Figures 5A and 6C). These observations indicated that SCC3, as a member of cohesin complex, had the function of inhibiting inter-sister chromatids exchange during meiosis. We also observed chromosome behaviors of *rec8* and *rec8 scc3* double mutants from diakinesis to anaphase I (Figure 6C). Both of these mutants contained defective chromosomes displaying a highly sticky phenotype from diakinesis to metaphase I, which is similar to the phenotype of non-homolog end joining (NHEJ). Moreover, chromosome fragmentation appeared in anaphase I, illustrating that meiotic DSBs were not well-repaired in *rec8* and *rec8 scc3*. In addition, DMC1 is also responsible for inter-sister exchange during meiosis in both arabidopsis and rice(Kurzbauer et al., 2012; Wang et al., 2016). To test whether DMC1 affects inter-sister repair process in *scc3*, we generated *dmc1 scc3* double mutant. The meiotic defects of *dmc1* and *dmc1 scc3* were identical from diakinesis to metaphase I, leading to 24 univalents (Figure 6C). Compared with *dmc1*, the sister chromatids of *dmc1 scc3* were completely separated in anaphase I and no chromosome fragmentation were observed. Taken together, meiotic DSBs in *scc3* is probably repaired by using sister chromatid as templates, and the inter-sister chromatids exchange in *scc3* is independent of DMC1.

The loading of SCC3 onto meiotic chromosomes depends on REC8

After observing that SCC3 is an axial element in meiosis, we evaluated whether its localization can be affected by other meiotic cohesin protein, specially REC8. Firstly, we investigated the number of γH2AX foci to explore the DSB formation in *rec8*, and found that the DSBs formation was normal in *rec8* (Figure 7A). In addition, DSBs ends resection factor COM1 (n=25 for 3 *rec8* mutants) and inter-homologue strand-invasion factor RAD51 (n=26 for 3 *rec8* mutants) fail to localize in *rec8*

(Figure 7A). Besides, we detected the distribution of SCC3 in *rec8*. we found no SCC3 signals in *rec8* mutants, suggesting REC8 affects the normal progression of SCC3 loading (n=36 for 3 *rec8* mutants). PAIR2 (n=28 for 3 *rec8* mutants) could only form short, interrupted stretches and few PAIR3 signals were detectable (n=32 for 3 *rec8* mutants). These results suggested that meiotic DSBs formation was normal in *rec8*, but DSBs ends resection and homologous recombination process were significantly defective. Thus, we speculated that the highly sticky chromosomes and dissociative chromosomes fragmentation from diakinesis to anaphase I in *rec8* was caused by COM1-mediated NHEJ pathway.

PAIR2 and PAIR3 localize on chromosome axes in rice, which is essential for the formation of synaptonemal complex installation. We further investigated the distribution of SCC3 in *pair2* and *pair3* mutants (Figure 7B). Specifically, SCC3 signals were normal in *pair2* and *pair3* mutants during meiosis. Moreover, SCC3 distribution was normal in other mutants that affect meiotic DSB formation (*spo11-1*), strand invasion and homology searching (*com1* and *dmc1*), and synaptonemal complex formation (*zep1*) (Figure 7B), indicating SCC3 localization is independent of the recombination process.

SCC3 interacts with RAD21.1

The cohesin complex is a ring-shaped protein complex where subunits interact with each other (Li et al., 2018a; Murayama and Uhlmann, 2015; Roig et al., 2014). To confirm this, we performed Y2H assays between several cohesin proteins. Surprisingly, we found SCC3 only interacts with RAD21.1 (Figure 7C), which was further confirmed in BiFC assays (Figure 7D). However, it is worth noting that SCC3 could not interact with other cohesin proteins, including REC8, SMC1 and SMC3 (Figure 7C), indicating that SCC3 could function directly in combination with RAD21.1 in the cohesin complex.

Previous studies showed cohesin regulates genes expression (Cuadrado et al.,

393 2015; Gligoris and Lowe, 2016; Remeseiro et al., 2012), we therefore investigated
394 expression levels of cohesin-related genes in wildtype and *scc3* spikelets using RT-
395 qPCR. Interestingly, we found cohesin subunits SCC1 and REC8, as well as
396 centromeric cohesin protector SGO1 were significantly downregulated in *scc3* (Figure
397 S10A). In contrast, the cohesin subunits SMC1 and SMC3, as well as lateral/central
398 elements PAIR3 and ZEP1 showed no differences in gene expression. The only
399 upregulated axial element in *scc3* spikelets was PAIR2.

400 We then investigated cohesin gene expression levels in axial/lateral elements
401 mutants (*pair2* and *pair3*) (Figure S10B), and found SMC3, SCC3 and SCC1 were
402 significantly downregulated compared to the wildtype. These findings suggested that
403 SCC3 may thus be involved in the transcriptional regulation of meiosis genes, while
404 axial elements affect cohesin proteins by regulating the expression levels of
405 associated genes.

406 Discussion

407 Chromosome segregation during mitosis and meiosis includes a series of highly
408 organized events, such as the formation of a cohesin complex containing different
409 subunits that play multiple functions (e.g., DSB repair, or gene expression regulation)
410 (Moronta-Gines et al., 2019; Nasmyth and Haering, 2009). Here, we show SCC3 is a
411 conserved cohesin subunit affecting vegetative growth and sister chromatid assembly
412 in both mitosis and meiosis. Crucially, our results also indicate SCC3 is a component
413 of LE/AE that is required for homologous pairing and synapsis during meiosis, which
414 is essential for the recombination process and CO formation. More importantly,
415 SCC3, as a member of cohesin complex, may inhibit inter-sister chromatids repair
416 during meiosis, which provides new insights between cohesin and inter-
417 sister/homolog recombination partner choice in meiotic DSBs repair.

418 Current cohesin complex research mainly focuses on mitosis because the
419 morphology of sister chromatids during meiosis is difficult to observe. In human

420 cells, sister chromatids separate in mitosis in the absence of the SCC3 homologues
421 SA1 and SA2. The former is required for telomere and arm cohesin, whereas the
422 latter is essential for centromere cohesin (Canudas and Smith, 2009). In rice, *SCC3*
423 has only a single copy, therefore we observed these all kinds of defects in *scc3*.
424 SCC3 is not only essential for the stability of sister chromatids cohesin but also plays
425 a role in loading cohesin onto chromosomes. In yeast *scc3*, the cohesin trimer
426 composed of SCC1, SMC1 and SMC3 remains intact. However, the trimer fails to
427 localize to chromosomes, probably because SCC3 helps maintaining the stability of
428 cohesin (Orgil et al., 2015; Pathania et al., 2021). Additionally, SCC3 contains a
429 conserved DNA binding domain in the SCC3-SCC1 subcomplex, which is required
430 for cohesin association to chromatin (Higashi et al., 2020). In yeast, the SCC3-SCC1
431 DNA-binding region recruits cohesin complexes to chromosomes and facilitates the
432 function of cohesin during mitotic cell division (Kulemzina et al., 2012; Li et al.,
433 2018a). These studies implied that SCC3-SCC1 interaction is necessary for cohesin
434 ring stability and for maintaining its association with DNA. In *Arabidopsis*, SCC3 is
435 also involved in vegetative growth of plants, but its role in mitosis remains unclear
436 (Chelysheva et al., 2005). Building from these previous observations, our study
437 demonstrated that SCC3 is encoded by a single gene that participates in early
438 cohesin formation in mitosis. In *scc3*, vegetative growth was severely inhibited. We
439 found that the replication process of sister chromatids during interphase was
440 abnormal in *scc3*, possibly because SCC3 is required for cohesin to stably bind to the
441 chromosomes. Also, we observed an increased distance between sister chromatids in
442 prometaphase, but sister chromatids remain partially dissociated not a complete
443 separation, indicating other cohesin subunits are still functional. Taken together, our
444 results suggest SCC3 is a conserved cohesin protein that plays a very important role
445 in mitosis.

446 SCC3 is also involved in meiotic chromosome structure and plays a crucial role
447 in homologous recombination and inter-sister chromatid repair during meiosis. In
448 vertebrates, SCC3 is encoded by two genes paralogues, including the meiosis-specific

449 subunit STAG3. In human *stag3*, SIM analysis showed the chromosome axes are
450 regionally separated and the synaptonemal complex is largely reduced (Biswas et al.,
451 2016; Fukuda et al., 2014; Hopkins et al., 2014; Llano et al., 2012). These
452 observations suggest STAG3 is required for synapsis between homologous
453 chromosomes. Compared to vertebrate cells, the morphology of meiocytes is more
454 readily observed during plant meiosis. In *Arabidopsis scc3*, a total loss of fertility is
455 associated with SCC3's role in meiosis, with unstable homologous pairing at
456 pachytene. SCC3 is also necessary for monopolar orientation of kinetochores at
457 meiosis I and the maintenance of centromeric cohesin at anaphase I (Chelysheva et
458 al., 2005). In other cohesin mutants, *Atscc2* is required for loading of the meiosis-
459 specific cohesin subunit REC8 (Wang et al., 2020), suggesting defects in cohesin-
460 related genes might impact the ability of the cohesin complex to bind chromosomes.
461 Accordingly, in meiosis, we found rice SCC3 has functions in the maintenance of
462 replication process of sister chromatids in preleptotene. SCC3 localizes between
463 homologous chromosomes as an important axial element during meiosis, ensuring
464 correct homologous pairing and synapsis. Meanwhile, SCC3 is required for normal
465 localization of DMC1, RAD51, ZIP4 and HEI10, which is essential for recombination
466 progress and CO formation. Our working model proposes SCC3 is a part of the
467 cohesin ring, and functions in specific association with SCC1 (Figures 8A).
468 Considering SCC3's role in cohesin and multiple meiotic functions, we speculate that
469 SCC3 may act as LE to stabilize loop boundaries to promote sister chromatids cohesin
470 during meiosis (Figure 8B). More importantly, meiotic homologous pairing and
471 synapsis are defective in *scc3*, and 24 univalents could be observed at diakinesis and
472 sister chromatids are completely separated at anaphase I with no chromosome
473 fragmentation, which illustrates that meiotic DSBs are well repaired and could only
474 use sister chromatids as a template to repair. Known meiotic components (COM1,
475 DMC1 and RAD51) can be present in *scc3* but apparently making no functional
476 contribution to homologous recombination, but these proteins could also have the
477 effect of creating a leading end that can search for an available inter-sister partner,
478 since DMC1 and RAD51 are also involved in inter-sister chromatids repair process.

We propose that, when cohesin is present, meiotic recombination exhibits inter-homolog bias to repair. Nonetheless, when cohesin is absent and homologous pairing is defective, recombination exhibits inter-sister bias to repair (Figure 8C). These observations imply that SCC3 acts as a component of cohesin complex, which could block inter-sister chromatids exchange during meiosis.

Cohesin is a multi-protein complex that plays a vital role establishing sister chromatid cohesin and high-order chromosome architecture in somatic and germ cells. However, distinct meiosis-specific subunits likely perform different functions (Cuadrado et al., 2015; Ishiguro, 2019; Schvarzstein et al., 2010). Our observations suggest that SCC3 and REC8 may play different roles during mitosis and meiosis. REC8 was considered a meiosis-specific protein, which played the role of SCC1 in meiosis to form cohesin complex. In this study, we found REC8 and SCC3 localization patterns were similar but not identical. Notably, REC8 was not present in mitotic cells. However, we found SCC3 is active in mitosis and meiosis, and may be involved in cohesin loading of the replication process of sister chromatids at preleptotene. It's worth noting that the mechanism of loading cohesin onto chromosomes in mitosis and meiosis was the same. Meiotic cohesin loaded onto chromosomes during interphase, probably when the sporogenous cell was replicating and acquired meiotic fate. This indicates REC8 is not involved in establishing cohesin at this instance. We also observed SCC3 signals at centromeres from diakinesis to metaphase I, but could not detect any REC8 at metaphase I. These different localization patterns also suggested they may have different functions in meiosis. Previous studies on Arabidopsis *rec8* mutants showed sticky chromosomes, and it was difficult to explain the reason of the phenotype (Cai et al., 2003; Lambing et al., 2020). Correspondingly, rice *rec8* meiocytes also contained defective chromosomes displaying a highly sticky phenotype from the diakinesis to metaphase I (Shao et al., 2011). Here, we found the chromosomes in *scc3* was not sticky as observed in *rec8* (Figure 6C). Meanwhile, the majority of meiotic proteins (including SCC3) failed to localize in *rec8*. This indicates the normal localization of SCC3 and other meiotic

proteins depends on REC8, which means REC8 may be a fundamental meiotic protein that is the prerequisite for other meiotic proteins loading. Also, the DSBs end processing and inter-sister/homolog strand-invasion are totally defective in *rec8*. Thus, we speculated that the sticky chromosomes in *rec8* may be caused by the NHEJ repair pathway (Figure 8C). The presented results provide that SCC3 acts as cohesin and stabilizes sister chromatid replication process in both mitosis and meiosis, but REC8 only functions in meiosis. Both proteins are independent of each other in mitosis, but related in meiosis, with REC8 representing a more important player in meiosis.

Material and methods

Meiotic chromosome preparation

Young rice panicles were fixed in Carnoy's solution (ethanol: acetic acid, 3: 1, v/v). Microsporocytes at different meiotic stages were squashed in an acetocarmine solution on glass slides. Moreover, the slides were covered with a coverslip and washed with 45% acetic acid from each side. Subsequently, the slides were frozen in liquid nitrogen for 10 seconds, and then the coverslip was removed as soon as possible ensuring sufficient cells were fixed on the slide. After ethanol gradient dehydration (70%, 90% and 100%), the slides with chromosome spreads were counterstained with 4',6-diamidino-2-phenylindole (DAPI, Vector Laboratories, Burlingame, CA, USA) solution. Chromosome behaviors were observed and captured using a ZEISS A2 microscope imaging system with a micro-charge-coupled (micro CCD) device camera.

Antibody production

To generate the antibody against SCC3, a 648 bp C-terminal fragment of *SCC3* complementary DNA (amino acids 900-1116) was amplified using primers SCC3-Ab-F and SCC3-Ab-R (Table S1). The PCR product was cloned into the expression vector pET-30a (Novagen, Madison, WI, USA). The fusion peptide expression and

534 purification were carried out as described previously (Miao et al., 2021). The
535 polyclonal antibody was raised from mouse and rabbit. Other antibodies were
536 generated in our laboratory previously.

537 **Immunofluorescence assay**

538 Fresh young panicles were fixed in 4% (w/v) paraformaldehyde for 30 min at room
539 temperature. Different meiotic stages of anthers were squashed in a drop of 1×PBS
540 solution on glass slides. After freezing in liquid nitrogen and ethanol dehydration,
541 slides were incubated with different combinations of diluted antibodies (1:100) in a
542 humid chamber at 37 °C for 2 h. Thereafter, the slides were washed with 1×PBS
543 solution three times and were further incubated for 1 h with the appropriate
544 fluorochrome-coupled secondary antibody, including fluorescein-isothiocyanate-
545 conjugated goat anti-mouse antibody (Southern Biotech, Birmingham, AL, USA),
546 rhodamine-conjugated goat anti-rabbit antibody (Southern Biotech), and AMCA-
547 conjugated goat anti-guinea pig antibody (Jackson ImmunoResearch, West Grove, PA,
548 USA). Slides were washed with 1×PBS solution three times and eventually stained
549 with DAPI. The immunofluorescence signals were analyzed and captured using a
550 ZEISS A2 microscope imaging system.

551 **Fluorescence *in situ* hybridization**

552 Young panicles of both wild-type and mutants were fixated in Carnoy's solution
553 (ethanol: acetic acid, 3: 1, v/v). The fluorescence *in situ* hybridization (FISH) analysis
554 was performed as a detailed protocol previously (Cheng, 2013). The pAtT4 clone
555 containing telomere repeats, the pTa794 clone containing 5S ribosomal RNA genes,
556 and the bulked oligonucleotide probes specific to chromosome 12 were used as probes
557 in FISH analysis. Rhodamine anti-digoxigenin was used for digoxigenin-labeled
558 probes. Chromosome images were captured using an Olympus (Shinjuku-ku, Tokyo,
559 Japan) BX51 fluorescence microscope with a micro CCD camera using software
560 IPLAB4.0 (BD Biosciences, San Jose, CA, USA).

561 **Yeast two-hybrid assay**

562 The yeast two-hybrid (Y2H) assays were conducted by the full-length CDSs of
563 *RAD21.1*, *SCC3*, *REC8*, *SMC1* and *SMC3* independently cloned into the pGBKT7 or
564 pGADT7 vector. Co-transformants were selected on SD/DDO (SD-Leu-Trp) medium
565 at 30 °C for 3-4 days. Positive interactions of transformants were selected on
566 SD/QDO (SD-Leu-Trp-His-Ade) medium containing aureobasidin A. All primers
567 used to construct plasmids are listed in Table S1. The detailed protocol was described
568 in the manufacturer's handbook (*Yeast protocols handbook*; PT3024-1; Clontech).

569 **BiFC assay**

570 To conduct BiFC assays, SCC3 and RAD21.1 were amplified by KOD-plus
571 polymerase and ligated into BiFC vectors, including pSCYNE (SCN) and pSCYCE
572 (SCC). The constructed plasmids were transformed into protoplasts extracted from the
573 young stem of rice etiolated seedlings. After incubation in the dark for 18 h at 28°C,
574 the CFP signals were captured under a confocal laser scanning microscope at an
575 excitation wavelength 405 nm (Leica TCS SP5, Wetzlar, Germany).

576 **Super-resolution structured illumination microscopy and image analysis**

577 Immunofluorescence assays were conducted by the procedures described above.
578 Meiotic cells with high-quality immunofluorescence signals were marked for
579 recording approximate X-Y positions using the ZEISS A2 microscope. Then these
580 cells were repositioned under the DeltaVision microscope (OMX^{TM} V4;
581 GEhealthcare, Chicago, IL, USA) and the super-resolution images were processed
582 with SoftWoRx (Applied Precision, Issaquah, WA, USA). And the distance between
583 axial elements was measured using I$_{MAGE}$J 1.37a software.

584 **RNA extraction and real-time PCR**

585 Real-time PCR assays were used to detect the expression patterns of *SCC3*. Total

586 RNA was extracted from different tissues in wild-type including root, stem, leaf,
587 sheath, spikelet, 2 cm long panicle, 2-3 cm long panicle, 3-5 cm long panicle, 5-7 cm
588 long panicle and 7 cm long panicle using TRIzol reagent. After digestion with RNase-
589 free DNaseI to remove genomic DNA, reverse transcription PCR was performed to
590 synthesize cDNA using SuperScript™ III Reverse Transcriptase by manufacturer's
591 protocol (Invitrogen). Quantitative real-time PCR assays were performed on the Bio-
592 Rad CFX96 instrument using Evagreen (Biotium, Freemont, CA, USA) with a
593 procedure of 98 °C 3min, 40 cycles of 98 °C 15s and 60 °C 20s. The *UBIQUITIN*
594 gene was used as an internal reference. Three biological repeats were performed for
595 each sample. Primers used for real-time PCR assays were listed in Table S1.

596 **Phylogenetic analysis**

597 The full-length amino acid sequence of SCC3 was selected as a template and searched
598 by the NCBI blastp tool to identify similar proteins among species. A detailed
599 protocol for further analysis has been reported previously (Li et al., 2018b; Ren et al.,
600 2018; Ren et al., 2020). Filtered sequences were downloaded and used for
601 constructing neighbor-joining trees by $M_{EGA}5$ software and processed with EvolvieW
602 (https://evolgenius.info/evolview/).

603 **Multiple sequence alignments**

604 Multiple alignments were performed using the online toolkit M_{AFFT}
605 (https://toolkit.tuebingen.mpg.de/mafft) and processed with $ESP_{RIPT}3$
606 (http://espript.ibcp.fr/ESPript/ESPript/) by previously detailed reported (Zhao et al.,
607 2021).

608 **Experimental model and subject details**

609 The rice *scc3* mutant was produced by CRISPR-Cas9 toolkit in *japonica* rice variety
610 Yandao 8. Primers used for CRISPR-Cas9 are listed in Table S1. Other meiosis
611 mutants *pair3* (Wuxiangjing 9), *pair2* (Nipponbare), *zep1* (Nipponbare), *rec8* (Yandao

8), *sgo1* (Yandao 8), *spo11-1* (Guangluai 4), *dmc1* (Nipponbare) have been previously described (Wang et al., 2016). Yandao 8 was used as the wild-type. All the rice plants were grown in a paddy field under natural rice-growing conditions.

Quantification and statistical analysis

At least three independent biological repeats were performed for each experiment. Values in Figures are means ± SD. The significant difference between the wild type and corresponding mutants was evaluated by two-tailed Student's t-test and $p < 0.05$ was considered as a criterion for judging statistically significant difference. The significance labeled in the Figures represents the following meanings: *, $p < 0.05$; **, $p < 0.01$; ***, $p < 0.001$; ****, $p < 0.0001$.

Acknoledgements

This work was supported by grants the National Natural Science Foundation of China (U2102219, 31930018 and 32201779).

Additional information

Author contributions

Z.C. and Y.Z. conceived the original screening and research plans; Y.Z., L.R., T.Z., H.Y., Y.M., L.C. and Y.S. performed most of the experiments; Y.Z., D.T. and Y.L. designed the experiments and analyzed the data; Y.Z. wrote the article; Z.C. supervised and complemented the writing.

Declaration of interests

The authors declare no competing interests.

Supplemental item

Figure S1 (related to Figure 1). Multiple sequence alignment of SCC3 with its homologs from three different species.

Figure S2 (related to Figure 1). Protein structure and phylogenetic tree analysis of SCC3.

Figure S3 (related to Figure 1). Multiple sequence alignment of SCC3 with its homologs from different species analyzed in evolutionary tree.

Figure S4 (related to Figure 1). Schematic representation of SCC3's mutation site.

Figure S5 (related to Figure 1). The expression pattern of SCC3 and plant phenotypic statistics of wildtype and *scc3* mutants.

Figure S6 (related to Figures 2 and 3). Immunolocalization of SCC3 and REC8 in *scc3* meiosis and mitosis.

Figure S7 (related to Figure 3). Immunolocalization of CENH3 and REC8 in wildtype from diakinesis to metaphase I.

Figure S8 (related to Figure 5). Chromosome behaviors of *spo11* and cytogenetic analysis of homologous pairing in wildtype and *scc3*.

Figure S9 (related to Figure 5). Immunolocalization of ZEP1, PAIR2 and PAIR3 in wildtype at zygotene.

Figure S10 (related to Figure 8). The expression levels of cohesin-related genes in wildtype and other mutants.

Table S1. List of primers used in this study.

References

Agostinho, A., Manneberg, O., van Schendel, R., Hernandez-Hernandez, A., Kouznetsova, A., Blom, H., Brismar, H., and Hoog, C. (2016). High density of REC8 constrains sister chromatid axes and prevents illegitimate synaptonemal complex formation. EMBO Rep *17*, 901-913.

Biswas, U., Hempel, K., Llano, E., Pendas, A., and Jessberger, R. (2016). Distinct Roles of Meiosis-Specific Cohesin Complexes in Mammalian Spermatogenesis. PLoS Genet *12*, e1006389.

Bolanos-Villegas, P., De, K., Pradillo, M., Liu, D., and Makaroff, C.A. (2017). In Favor of Establishment: Regulation of Chromatid Cohesion in Plants. Front Plant Sci *8*, 846.

Cai, X., Dong, F., Edelmann, R.E., and Makaroff, C.A. (2003). The Arabidopsis SYN1 cohesin protein is required for sister chromatid arm cohesion and homologous chromosome pairing. J Cell Sci *116*, 2999-3007.

Canudas, S., and Smith, S. (2009). Differential regulation of telomere and centromere cohesion by the Scc3 homologues SA1 and SA2, respectively, in human cells. J Cell Biol *187*, 165-173.

667 Casa, V., Moronta Gines, M., Gade Gusmao, E., Slotman, J.A., Zirkel, A., Josipovic, N., Oole, E., van,
668 I.W.F.J., Houtsmuller, A.B., Papantonis, A.*, et al.* (2020). Redundant and specific roles of cohesin STAG
669 subunits in chromatin looping and transcriptional control. Genome Res *30*, 515-527.
670 Chelysheva, L., Diallo, S., Vezon, D., Gendrot, G., Vrielynck, N., Belcram, K., Rocques, N., Marquez-
671 Lema, A., Bhatt, A.M., Horlow, C.*, et al.* (2005). AtREC8 and AtSCC3 are essential to the monopolar
672 orientation of the kinetochores during meiosis. J Cell Sci *118*, 4621-4632.
673 Cheng, Z. (2013). Analyzing meiotic chromosomes in rice. Methods Mol Biol *990*, 125-134.
674 Cuadrado, A., Remeseiro, S., Grana, O., Pisano, D.G., and Losada, A. (2015). The contribution of
675 cohesin-SA1 to gene expression and chromatin architecture in two murine tissues. Nucleic Acids Res
676 *43*, 3056-3067.
677 Fujiwara, Y., Horisawa-Takada, Y., Inoue, E., Tani, N., Shibuya, H., Fujimura, S., Kariyazono, R., Sakata, T.,
678 Ohta, K., Araki, K.*, et al.* (2020). Meiotic cohesins mediate initial loading of HORMAD1 to the
679 chromosomes and coordinate SC formation during meiotic prophase. PLoS Genet *16*, e1009048.
680 Fukuda, T., Fukuda, N., Agostinho, A., Hernandez-Hernandez, A., Kouznetsova, A., and Hoog, C. (2014).
681 STAG3-mediated stabilization of REC8 cohesin complexes promotes chromosome synapsis during
682 meiosis. EMBO J *33*, 1243-1255.
683 Gligoris, T., and Lowe, J. (2016). Structural Insights into Ring Formation of Cohesin and Related Smc
684 Complexes. Trends Cell Biol *26*, 680-693.
685 Gryaznova, Y., Keating, L., Touati, S.A., Cladiere, D., El Yakoubi, W., Buffin, E., and Wassmann, K. (2021).
686 Kinetochore individualization in meiosis I is required for centromeric cohesin removal in meiosis II.
687 EMBO J *40*, e106797.
688 Higashi, T.L., Eickhoff, P., Sousa, J.S., Locke, J., Nans, A., Flynn, H.R., Snijders, A.P., Papageorgiou, G.,
689 O'Reilly, N., Chen, Z.A.*, et al.* (2020). A Structure-Based Mechanism for DNA Entry into the Cohesin
690 Ring. Mol Cell *79*, 917-933 e919.
691 Hong, S., Sung, Y., Yu, M., Lee, M., Kleckner, N., and Kim, Keun P. (2013). The Logic and Mechanism of
692 Homologous Recombination Partner Choice. Molecular Cell *51*, 440-453.
693 Hopkins, J., Hwang, G., Jacob, J., Sapp, N., Bedigian, R., Oka, K., Overbeek, P., Murray, S., and Jordan,
694 P.W. (2014). Meiosis-specific cohesin component, Stag3 is essential for maintaining centromere
695 chromatid cohesion, and required for DNA repair and synapsis between homologous chromosomes.
696 PLoS Genet *10*, e1004413.
697 Ishiguro, K., and Watanabe, Y. (2007). Chromosome cohesion in mitosis and meiosis. J Cell Sci *120*,
698 367-369.
699 Ishiguro, K.I. (2019). The cohesin complex in mammalian meiosis. Genes Cells *24*, 6-30.
700 Kagey, M.H., Newman, J.J., Bilodeau, S., Zhan, Y., Orlando, D.A., van Berkum, N.L., Ebmeier, C.C.,
701 Goossens, J., Rahl, P.B., Levine, S.S.*, et al.* (2010). Mediator and cohesin connect gene expression and
702 chromatin architecture. Nature *467*, 430-435.
703 Klein, F., Mahr, P., Galova, M., Buonomo, S.B.C., Michaelis, C., Nairz, K., and Nasmyth, K. (1999). A
704 Central Role for Cohesins in Sister Chromatid Cohesion, Formation of Axial Elements, and
705 Recombination during Yeast Meiosis. Cell *98*, 91-103.
706 Kulemzina, I., Schumacher, M.R., Verma, V., Reiter, J., Metzler, J., Failla, A.V., Lanz, C., Sreedharan, V.T.,
707 Ratsch, G., and Ivanov, D. (2012). Cohesin rings devoid of Scc3 and Pds5 maintain their stable
708 association with the DNA. PLoS Genet *8*, e1002856.
709 Kurzbauer, M.-T., Uanschou, C., Chen, D., and Schlögelhofer, P. (2012). The Recombinases DMC1 and
710 RAD51 Are Functionally and Spatially Separated during Meiosis in Arabidopsis. The Plant Cell *24*, 2058-

711 2070.
712 Lambing, C., Tock, A.J., Topp, S.D., Choi, K., Kuo, P.C., Zhao, X., Osman, K., Higgins, J.D., Franklin, F.C.H.,
713 and Henderson, I.R. (2020). Interacting Genomic Landscapes of REC8-Cohesin, Chromatin, and Meiotic
714 Recombination in Arabidopsis. Plant Cell *32*, 1218-1239.
715 Lara-Pezzi, E., Pezzi, N., Prieto, I., Barthelemy, I., Carreiro, C., Martinez, A., Maldonado-Rodriguez, A.,
716 Lopez-Cabrera, M., and Barbero, J.L. (2004). Evidence of a transcriptional co-activator function of
717 cohesin STAG/SA/Scc3. J Biol Chem *279*, 6553-6559.
718 Li, Y., Muir, K.W., Bowler, M.W., Metz, J., Haering, C.H., and Panne, D. (2018a). Structural basis for Scc3-
719 dependent cohesin recruitment to chromatin. Elife *7*.
720 Li, Y., Qin, B., Shen, Y., Zhang, F., Liu, C., You, H., Du, G., Tang, D., and Cheng, Z. (2018b). HEIP1
721 regulates crossover formation during meiosis in rice. Proc Natl Acad Sci U S A *115*, 10810-10815.
722 Llano, E., Herran, Y., Garcia-Tunon, I., Gutierrez-Caballero, C., de Alava, E., Barbero, J.L., Schimenti, J.,
723 de Rooij, D.G., Sanchez-Martin, M., and Pendas, A.M. (2012). Meiotic cohesin complexes are essential
724 for the formation of the axial element in mice. J Cell Biol *197*, 877-885.
725 Mercier, R., Mezard, C., Jenczewski, E., Macaisne, N., and Grelon, M. (2015). The molecular biology of
726 meiosis in plants. Annu Rev Plant Biol *66*, 297-327.
727 Miao, Y., Shi, W., Wang, H., Xue, Z., You, H., Zhang, F., Du, G., Tang, D., Li, Y., Shen, Y.*, et al.* (2021).
728 Replication protein A large subunit (RPA1a) limits chiasma formation during rice meiosis. Plant Physiol
729 *187*, 1605-1618.
730 Michaelis, C., Ciosk, R., and Nasmyth, K. (1997). Cohesins: Chromosomal proteins that prevent
731 premature separation of sister chromatids. Cell *91*, 35-45.
732 Moronta-Gines, M., van Staveren, T.R.H., and Wendt, K.S. (2019). One ring to bind them - Cohesin's
733 interaction with chromatin fibers. Essays Biochem *63*, 167-176.
734 Murayama, Y., and Uhlmann, F. (2015). DNA Entry into and Exit out of the Cohesin Ring by an
735 Interlocking Gate Mechanism. Cell *163*, 1628-1640.
736 Nasmyth, K., and Haering, C.H. (2009). Cohesin: its roles and mechanisms. Annu Rev Genet *43*, 525-
737 558.
738 Ogushi, S., Rattani, A., Godwin, J., Metson, J., Schermelleh, L., and Nasmyth, K. (2021). Loss of sister
739 kinetochore co-orientation and peri-centromeric cohesin protection after meiosis I depends on
740 cleavage of centromeric REC8. Dev Cell *56*, 3100-3114 e3104.
741 Orgil, O., Matityahu, A., Eng, T., Guacci, V., Koshland, D., and Onn, I. (2015). A conserved domain in the
742 scc3 subunit of cohesin mediates the interaction with both mcd1 and the cohesin loader complex.
743 PLoS Genet *11*, e1005036.
744 Pathania, A., Liu, W., Matityahu, A., Irudayaraj, J., and Onn, I. (2021). Chromosome loading of cohesin
745 depends on conserved residues in Scc3. Curr Genet.
746 Phipps, J., and Dubrana, K. (2022). DNA Repair in Space and Time: Safeguarding the Genome with the
747 Cohesin Complex. Genes *13*.
748 Remeseiro, S., Cuadrado, A., Gomez-Lopez, G., Pisano, D.G., and Losada, A. (2012). A unique role of
749 cohesin-SA1 in gene regulation and development. EMBO J *31*, 2090-2102.
750 Ren, L., Tang, D., Zhao, T., Zhang, F., Liu, C., Xue, Z., Shi, W., Du, G., Shen, Y., Li, Y.*, et al.* (2018). OsSPL
751 regulates meiotic fate acquisition in rice. New Phytol *218*, 789-803.
752 Ren, L., Zhao, T., Zhang, L., Du, G., Shen, Y., Tang, D., Li, Y., Luo, Q., and Cheng, Z. (2020). Defective
753 Microspore Development 1 is required for microspore cell integrity and pollen wall formation in rice.
754 Plant J *103*, 1446-1459.

755 Ren, L., Zhao, T., Zhao, Y., Du, G., Yang, S., Mu, N., Tang, D., Shen, Y., Li, Y., and Cheng, Z. (2021). The E3
756 ubiquitin ligase DESYNAPSIS1 regulates synapsis and recombination in rice meiosis. Cell Rep *37*,
757 109941.
758 Roig, M.B., Lowe, J., Chan, K.L., Beckouet, F., Metson, J., and Nasmyth, K. (2014). Structure and
759 function of cohesin's Scc3/SA regulatory subunit. FEBS Lett *588*, 3692-3702.
760 Sanchez-Moran, E., Santos, J.-L., Jones, G.H., and Franklin, F.C.H. (2007). ASY1 mediates AtDMC1-
761 dependent interhomolog recombination during meiosis in Arabidopsis. Genes & Development *21*,
762 2220-2233.
763 Schvarzstein, M., Wignall, S.M., and Villeneuve, A.M. (2010). Coordinating cohesion, co-orientation,
764 and congression during meiosis: lessons from holocentric chromosomes. Genes Dev *24*, 219-228.
765 Shao, T., Tang, D., Wang, K., Wang, M., Che, L., Qin, B., Yu, H., Li, M., Gu, M., and Cheng, Z. (2011).
766 OsREC8 is essential for chromatid cohesion and metaphase I monopolar orientation in rice meiosis.
767 Plant Physiol *156*, 1386-1396.
768 Toth, A., Rabitsch, K.P., Galova, M., Schleiffer, A., Buonomo, S.B., and Nasmyth, K. (2000). Functional
769 genomics identifies monopolin: a kinetochore protein required for segregation of homologs during
770 meiosis i. Cell *103*, 1155-1168.
771 Wang, H., Hu, Q., Tang, D., Liu, X., Du, G., Shen, Y., Li, Y., and Cheng, Z. (2016). OsDMC1 Is Not Required
772 for Homologous Pairing in Rice Meiosis. Plant Physiology *171*, 230-241.
773 Wang, H., Xu, W., Sun, Y., Lian, Q., Wang, C., Yu, C., He, C., Wang, J., Ma, H., Copenhaver, G.P.*, et al.*
774 (2020). The cohesin loader SCC2 contains a PHD finger that is required for meiosis in land plants. PLoS
775 Genet *16*, e1008849.
776 Wang, M., Tang, D., Luo, Q., Jin, Y., Shen, Y., Wang, K., and Cheng, Z. (2012). BRK1, a Bub1-related
777 kinase, is essential for generating proper tension between homologous kinetochores at metaphase I of
778 rice meiosis. Plant Cell *24*, 4961-4973.
779 Wang, M., Tang, D., Wang, K., Shen, Y., Qin, B., Miao, C., Li, M., and Cheng, Z. (2011). OsSGO1
780 maintains synaptonemal complex stabilization in addition to protecting centromeric cohesion during
781 rice meiosis. Plant J *67*, 583-594.
782 Watanabe, Y. (2005). Sister chromatid cohesion along arms and at centromeres. Trends Genet *21*, 405-
783 412.
784 Watanabe, Y., and Nurse, P. (1999). Cohesin Rec8 is required for reductional chromosome segregation
785 at meiosis. Nature *400*, 461-464.
786 Zhang, F., Ma, L., Zhang, C., Du, G., Shen, Y., Tang, D., Li, Y., Yu, H., Ma, B., and Cheng, Z. (2020). The
787 SUN Domain Proteins OsSUN1 and OsSUN2 Play Critical but Partially Redundant Roles in Meiosis. Plant
788 Physiol *183*, 1517-1530.
789 Zhao, T., Ren, L., Chen, X., Yu, H., Liu, C., Shen, Y., Shi, W., Tang, D., Du, G., Li, Y.*, et al.* (2018). The
790 OsRR24/LEPTO1 Type-B Response Regulator is Essential for the Organization of Leptotene
791 Chromosomes in Rice Meiosis. Plant Cell *30*, 3024-3037.
792 Zhao, T., Ren, L., Zhao, Y., You, H., Zhou, Y., Tang, D., Du, G., Shen, Y., Li, Y., and Cheng, Z. (2021).
793 Reproductive cells and peripheral parietal cells collaboratively participate in meiotic fate acquisition in
794 rice anthers. Plant J *108*, 661-671.
795

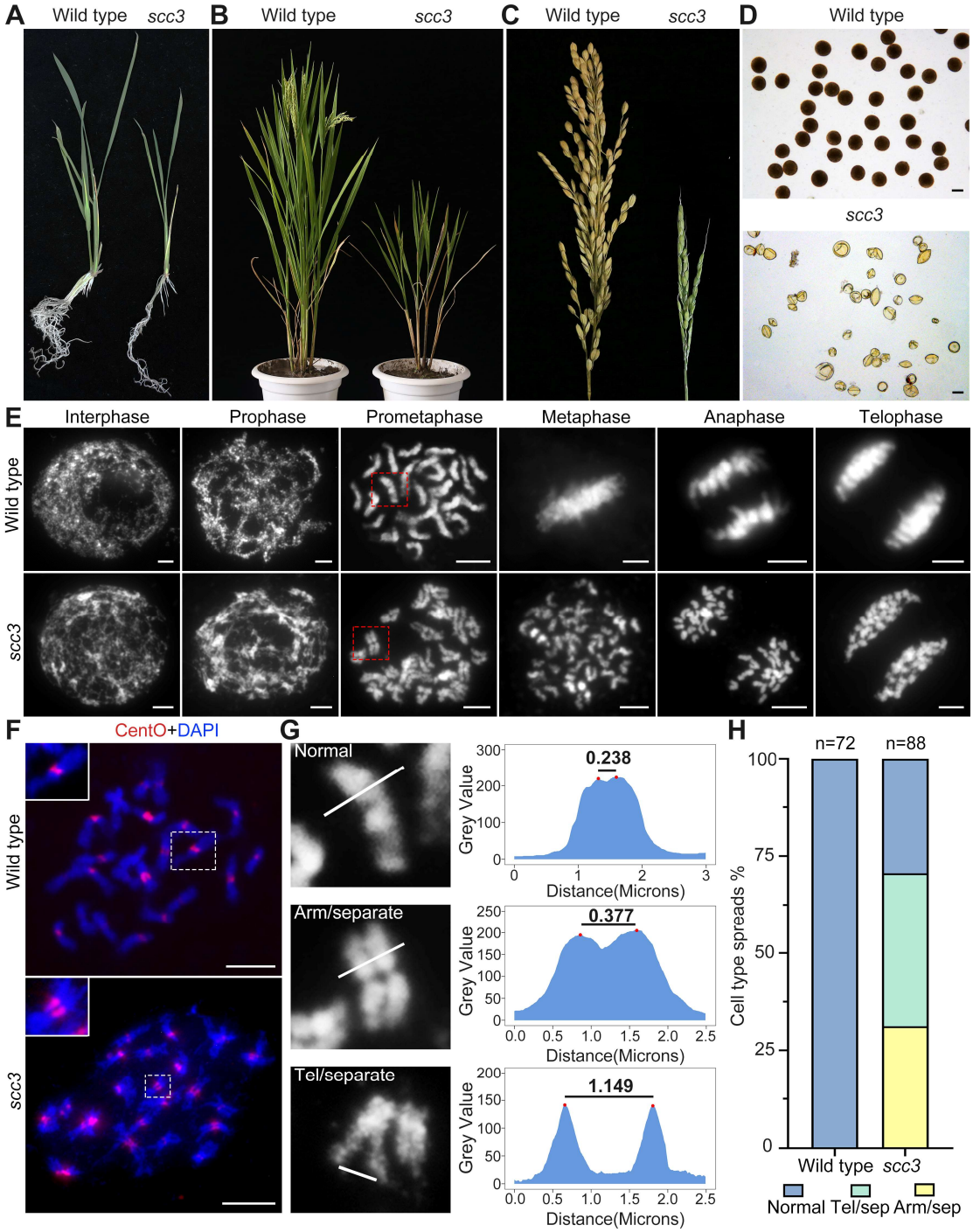

Figure 1. SCC3 is required for sister chromatid cohesin during mitosis

(A) Comparison between seedlings and root tips in wildtype and *scc3*.

(B) Comparison between wildtype and *scc3* mutant plants.

(C) Comparison between wildtype and *scc3* mutant panicles.

(D) Pollen grains stained in 1% I2-KI solution in wildtype and *scc3*. Bars, 50 μm.

(E) The chromosome behaviors of root tip cells in wildtype and *scc3*, stained with DAPI. Individual chromosomes are marked by red boxes. The distance between the sister

chromatids increased significantly at prometaphase, and the sister chromatids separated in advance at metaphase in *scc3*. Bars, 5 μm.

(F) FISH analysis of mitotic cells with centromere-specific fluorescently labeled probes in the wildtype and *scc3*. The distance between centromeres increased significantly in *scc3*. CentO (red) signals indicate centromeres. Chromosomes were stained with DAPI (blue). Bars, 5μm.

(G) The distance between sister chromatids in different mitotic chromosomes. In normal condition, two sister chromatids form tight stick. In *scc3*, the distance between chromosome arms and telomeres were increased significantly. Curve diagrams show the distance between the arms and the telomeres as measured by IMAGEJ. Bars, 1 μm.

(H) Graphical representation of the frequency of each type of chromosome morphology. The classification was assigned when >50% chromosomes in a spread displayed the indicated morphology.

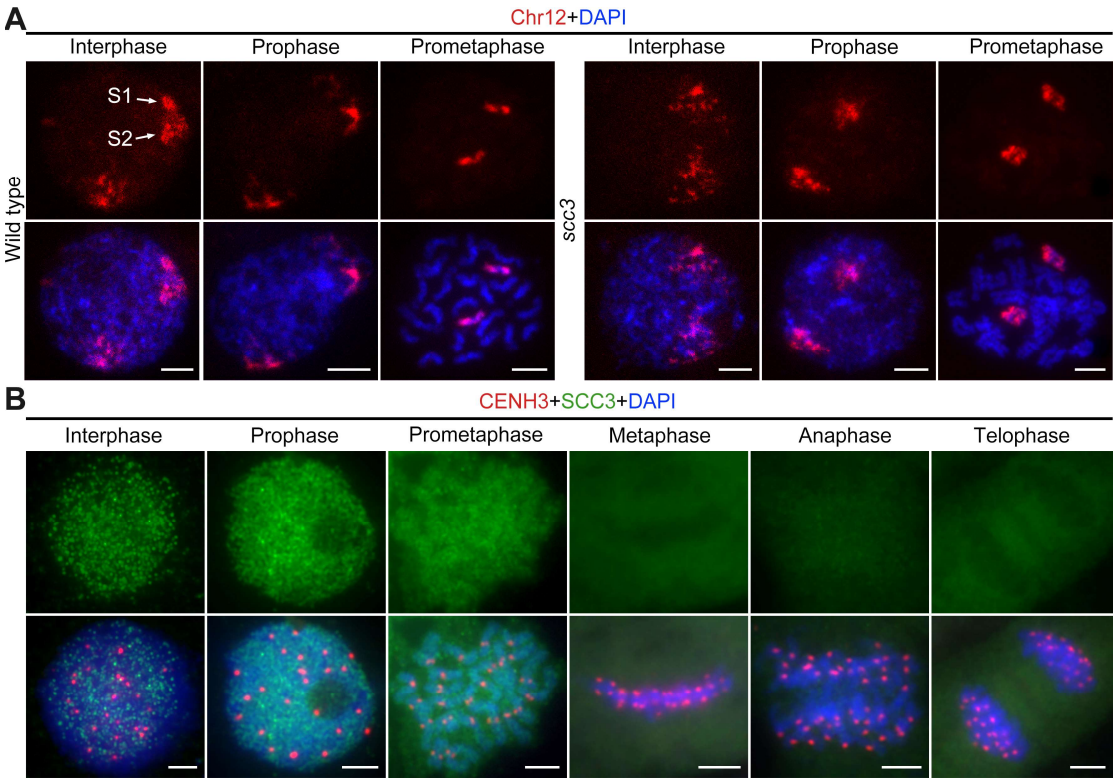

Figure 2. SCC3 affects the replication process of sister chromatids during mitosis

(A) The dynamic process of chromosome replication in early mitosis as revealed by pooled oligos specific to chromosome 12 (red). In the wildtype, S1 and S2 indicate the sister chromatids that are replicating. However, in *scc3* sister chromatids exhibit many chromosome fragmentation during replication at interphase. Mitotic chromosomes in wildtype and *scc3* were stained with DAPI (blue). Bars, 5 μm.

(B) The loading pattern of SCC3 (green, from mouse) and CENH3 (red, from rabbit) in wildtype root tip cells. Chromosomes were stained with DAPI (blue). Bars, 5 μm.

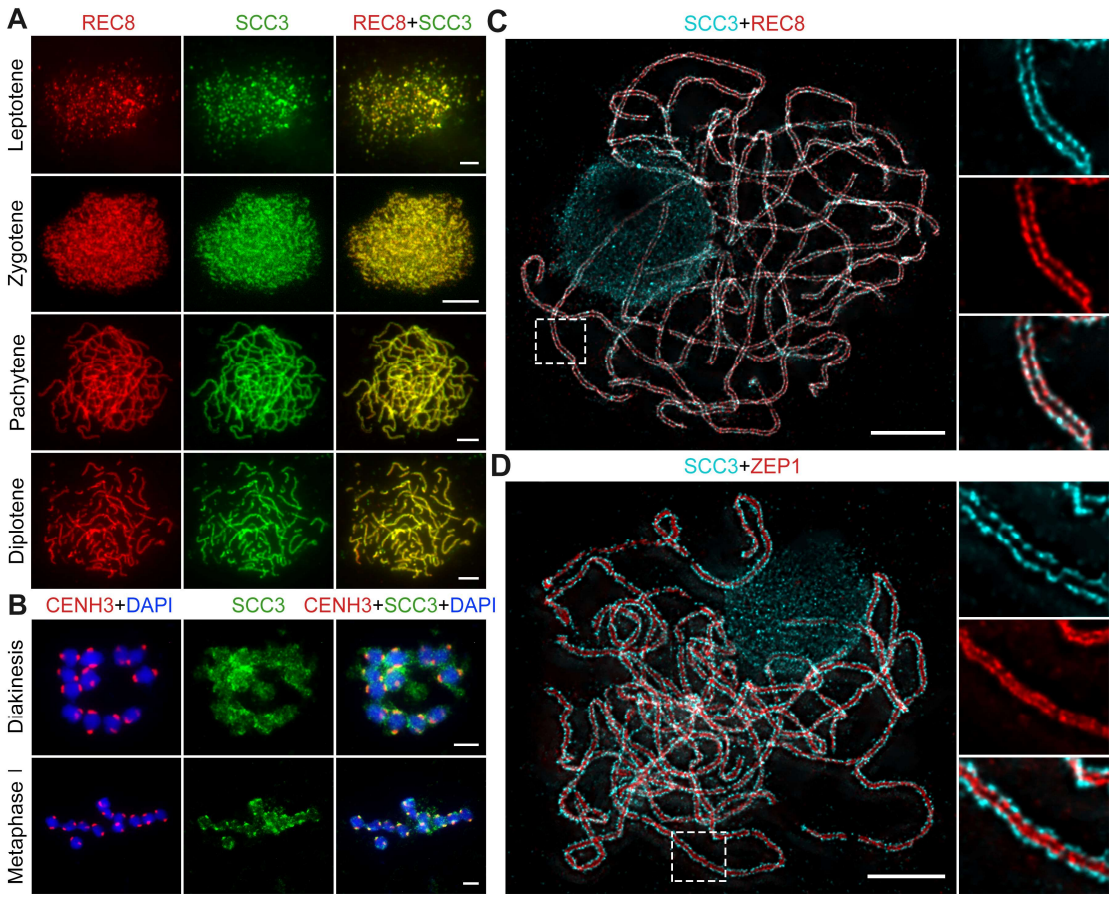

Figure 3. SCC3 is an axial element during meiosis

(A) In meiosis, SCC3 (green, from mouse) colocalizes with REC8 (red, from rabbit) from the leptotene to diplotene. Bars, 5 μm.

(B) During diakinesis and metaphase I, SCC3 (green, from mouse) gradually dispersed and finally retained in the centromeres indicated by CENH3 (red, from rabbit). Chromosomes were stained with DAPI (blue). Bars, 5 μm.

(C) Immunostaining of SCC3 (cyan, from mouse) and REC8 (red, from rabbit) in wildtype meiocytes at pachytene. Two parallel linear SCC3 signals colocalize with the REC8 linear signals, indicating chromosomal axial elements. Magnified images of the blocked regions are shown on the right. Bars, 5 μm.

(D) Immunostaining of SCC3 (cyan, from mouse) and ZEP1 (red, from rabbit) in wildtype meiocytes at pachytene. Two linear SCC3 signals wrap the ZEP1 signals, indicating chromosomal central elements are wrapped by axial elements. Magnified images of the blocked regions are shown on the right. Bars, 5 μm.

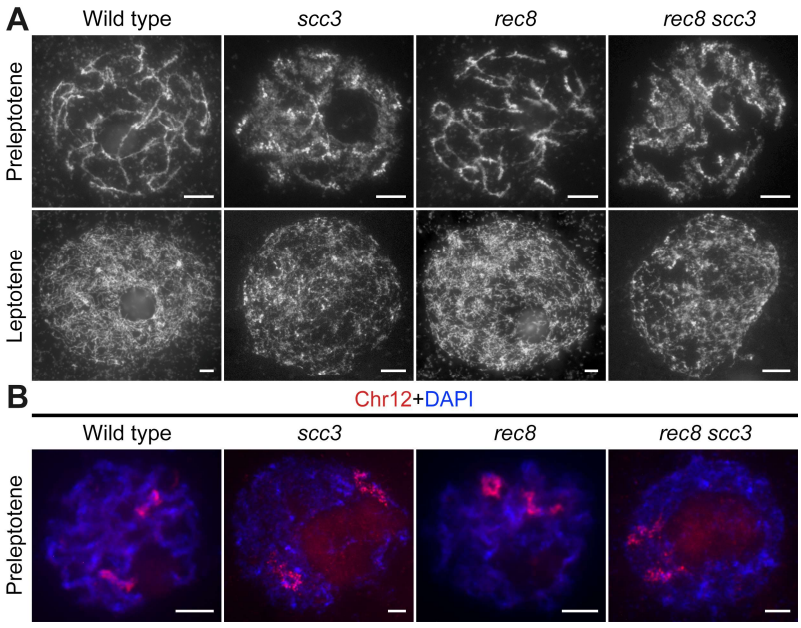

Figure 4. SCC3 is required for sister chromatid cohesin in early meiosis

(A) Meiocyte chromosome morphology at the preleptotene and leptotene in wildtype, *scc3*, *rec8* and *rec8 scc3*. Chromosomes at preleptotene exhibited a hairy rodlike appearance and formed thin threads at leptotene in wildtype. However, chromosomes in *scc3* were dispersed with blurred outlines and failed to from thin threads at leptotene. Bars, 5 μm.

(B) The process of chromosome replication in preleptotene is revealed by pooled oligos specific to chromosome 12 (red). Preleptotene chromosomes in wildtype, *scc3*, *rec8* and *rec8 scc3*. Chromosomes were stained with DAPI (blue). Bars, 5 μm.

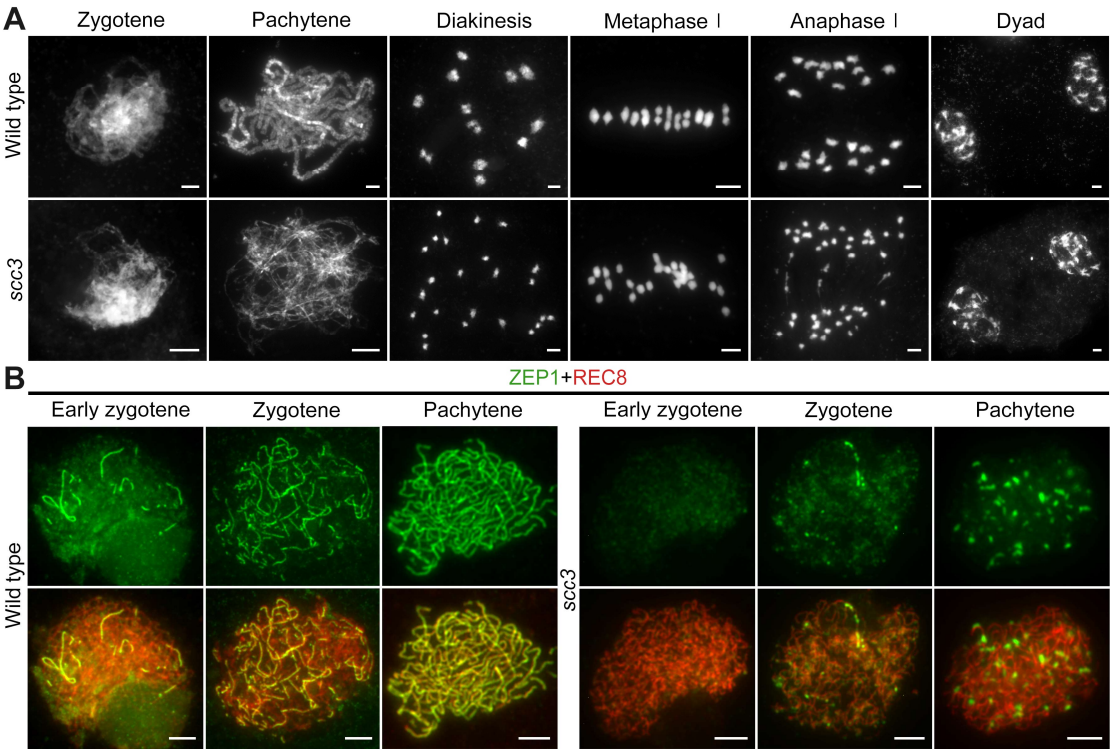

Figure 5. Homologous pairing and synapsis are disturbed in *scc3*

(A) Meiotic chromosome behavior in wildtype and *scc3*. Bars, 5 μm.

(B) Immunolocalization of ZEP1 (green, from mouse) and REC8 (red, from rabbit) in wildtype and scc3 meiocytes. ZEP1 was severely suppressed from zygotene to late pachytene in scc3. Bars, 5 μm.

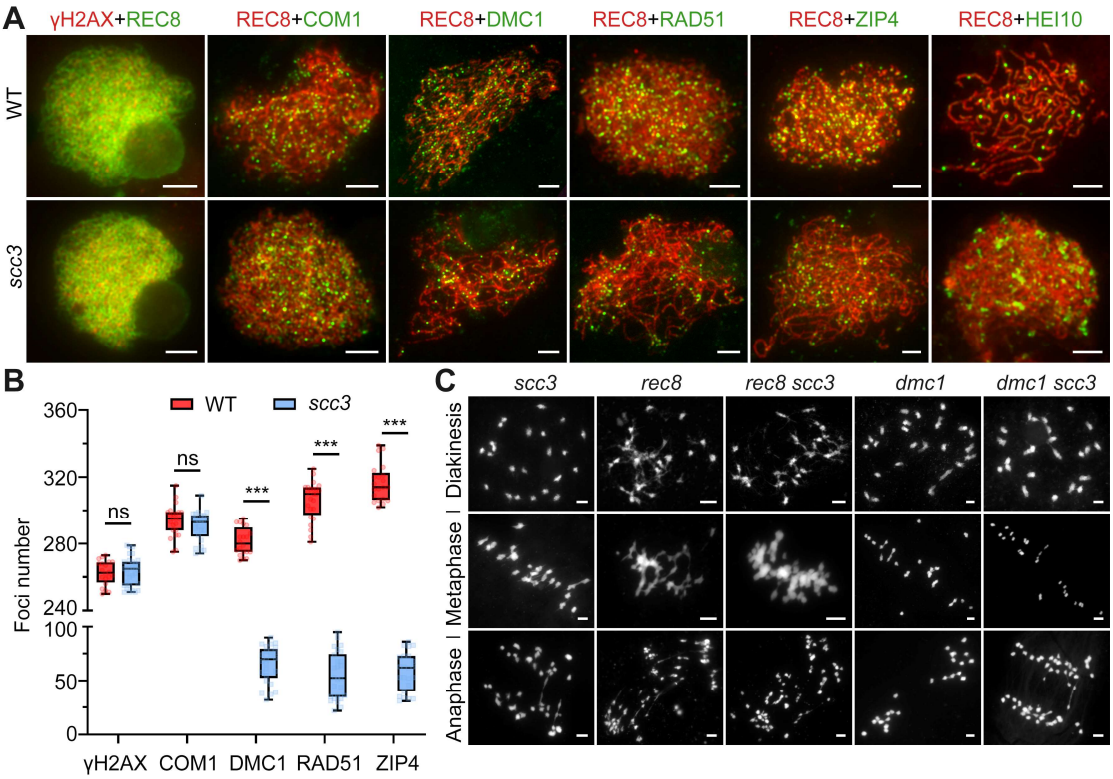

Figure 6. SCC3 affects recombination progress and CO formation

(A) Immunolocalization of histone γH2AX phosphorylation (red), COM1 (green, from mouse), DMC1 (green, from mouse), RAD51 (green, from rabbit), ZIP4 (green, from mouse) and HEI10 (green, from mouse) in wildtype and *scc3*. REC8 (red, from mouse and rabbit) signals were used to visualize chromosome axes. Bars, 5 μm.

(B) Box scatter plot of histone γH2AX phosphorylation, COM1, DMC1, RAD51 and ZIP4 in wildtype and *scc3*. No difference of histone γH2AX phosphorylation and COM1 were shown between the wildtype and *scc3*. DMC1, RAD51 and ZIP4 foci were significantly decreased in *scc3* compared with wildtype. Values are means ± SD. *** represents $P < 0.001$, two-tailed Student's *t*-tests was performed.

(C) Chromosome behavior in *scc3*, *rec8*, *rec8 scc3*, *dmc1* and *dmc1 scc3* from diakinesis to anaphase I. Bars, 5 μm.

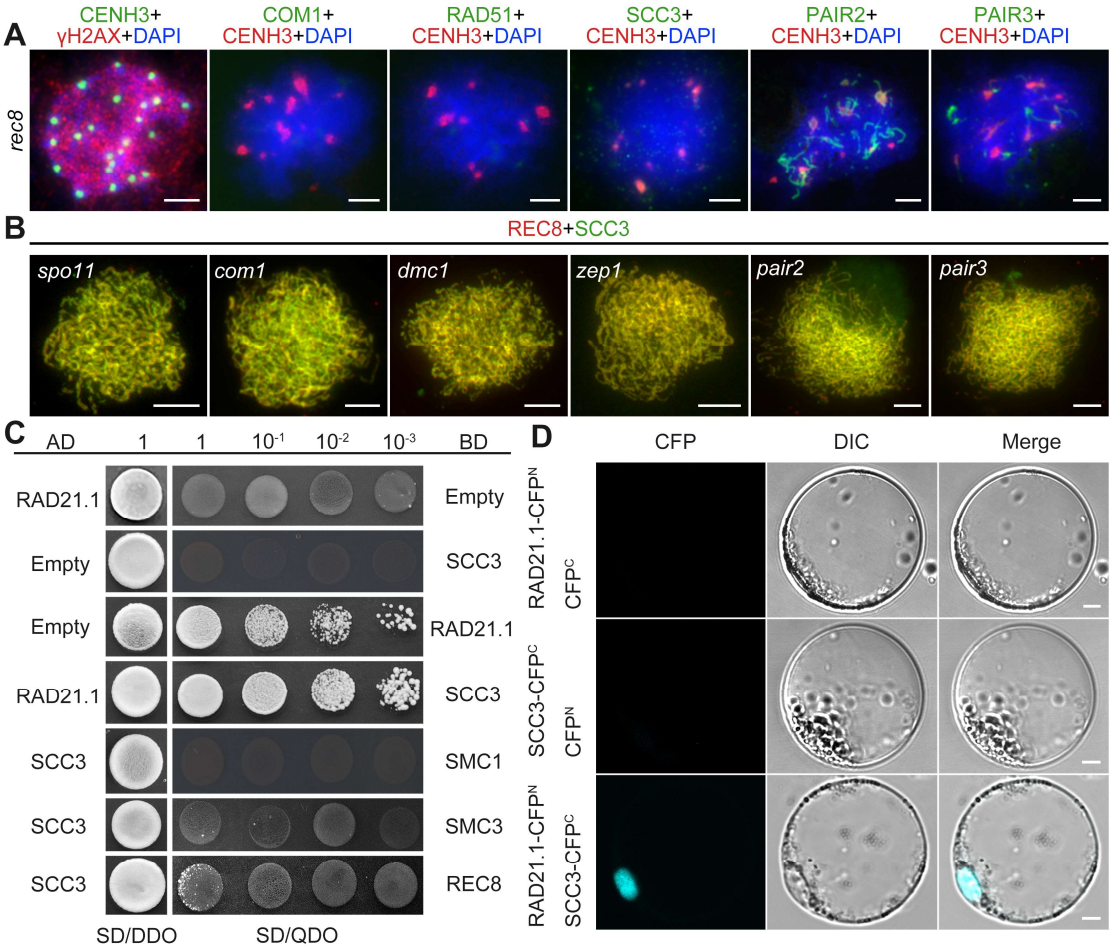

Figure 7. SCC3 loading onto meiotic chromosomes depends on REC8

(A) Immunolocalization of γH2AX (red, from rabbit), COM1 (green, from mouse), RAD51 (green, from rabbit), SCC3 (green, from mouse), PAIR2 (green, from rabbit) and PAIR3 (green, from rabbit) in *rec8* meiocytes at zygotene. CENH3 (red and green, from rabbit and mouse) was used to indicate the centromeres. Bars, 5 μm.

(B) Immunolocalization of REC8 (red, from rabbit) and SCC3 (green, from mouse) in *spo11*, *com1*, *dmc1*, *zep1*, *pair2* and *pair3* meiocytes at zygotene. Bars, 5 μm.

(C) SCC3 interacts with RAD21.1 in yeast-two-hybrid assays. Interactions between bait and prey were examined on SD/DDO (SD-Leu-Trp) control media and SD/QDO (SD-Ade-His-Leu-Trp) selective media. AD, prey vector; BD, bait vector.

(D) Bimolecular fluorescence complementation assays show the interactions between SCC3 and RAD21.1 in rice protoplasts. Bars, 5 μm.

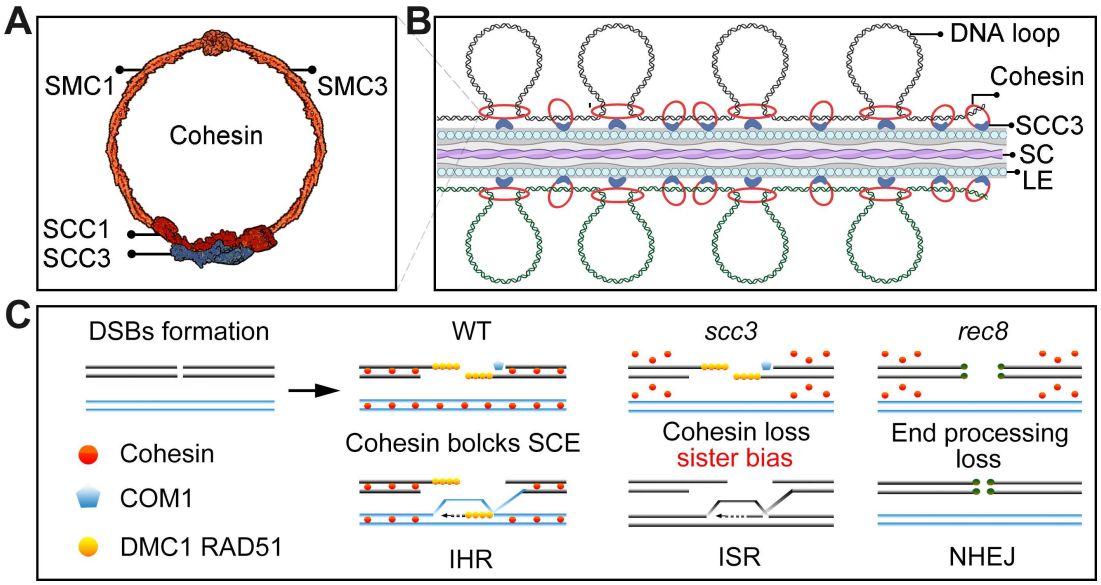

Figure 8. SCC3 acts as the cohesin and inhibits inter-sister chromatids repair during rice meiosis

(A) Structure model of the cohesin complex. The SCC3 subunit is associated with the middle region of SCC1.

(B) During meiosis, SCC3's localization pattern probably changes to the root of DNA loop with lateral elements (LE), which wraps synaptonemal complex (SC). This indicates SCC3 is a meiotic LE essential for homologous chromosome pairing and synapsis, also affects recombination progress and CO formation.

(C) Meiotic recombination exhibits an intrinsic and mechanistical default towards selection of homolog bias in wildtype. Cohesin is responsible for the connection of sister chromatids intervening in this mechanism to inhibit recombination into use of sisters. However, in *scc3*, sister bias is required, with the defects of homologous pairing and synapsis. This outcome may be achieved by the residue function of DMC1 and RAD51 promoting DSBs end association with sister. While this situation in *rec8* is quite different with most meiotic proteins fail to localize, thus forced to NHEJ repair pathway causing the sticky chromosomes and fragmentation.